Inorganic Chemistry

ARTICLE

pubs.acs.org/IC

Experimental and Theoretical Studies of the Vibrational and Electronic Spectra of a Lanthanide Ion at a Site of T_h Symmetry: Pr^{3+} in $Cs_2NaPr(NO_2)_6$

Wenyu Li,[†] Lixin Ning,[‡] Michèle D. Faucher,[§] and Peter A. Tanner*[,†]

[†]Department of Biology and Chemistry, City University of Hong Kong, Tat Chee Avenue, Kowloon, Hong Kong, People's Republic of China

[‡]Department of Physics, Anhui Normal University, Wuhu, Anhui 241000, People's Republic of China

Supporting Information

ABSTRACT: The Pr^{3+} ion in $Cs_2NaPr(NO_2)_6$ is situated at a site of T_h symmetry with 12-coordination to O atoms of bidentate nitrito groups. First-principles calculations of the vibrational modes of the complex were carried out using the density functional theory with the generalized gradient approximation Perdew−Burke−Ernzerhof exchange-correlation functional. The calculations that treated the Pr^{3+} 4f electrons as valence electrons showed better agreement with the experimental vibrational assignments compared with those treating the 4f electrons a part of the inner core. The $^1D_2 \rightarrow {}^3H_4$ emission spectra of $Cs_2NaPr(NO_2)_6$ at 7 K enabled assignments to be made for the crystal-field (CF) levels of the ground-state multiplet. The emission of the dilute system $Cs_2NaY(NO_2)_6$:Pr^{3+} was dominated by NO_2^- triplet emission, which was quenched at elevated temperatures by energy transfer to trace Eu^{3+} impurity. From magnetic dipole calculations and the vibronic fingerprint, detailed assignments are given for the complex 10 K electronic absorption spectrum of $Cs_2NaPr(NO_2)_6$ between 3940 and 18800 cm^{-1}, and the derived Pr^{3+} $4f^2$ energy-level data set has been fitted by calculation. By comparison with $Cs_2NaPrCl_6$, the fourth-order CF parameter in $Cs_2NaPr(NO_2)_6$ is relatively small so that interaction with a 4*f*np configuration is not important. From the NO_2^- absorption bands above 20 000 cm^{-1}, the N−O bond length change upon excitation is small, whereas the angle O−N−O opens by more than 10° in the triplet state. By contrast to the NO_2^- internal vibration frequencies, which except for the wagging mode show only minor changes with the environment, the triplet-state energy shows a linear decrease with an increase of the lanthanide (Ln^{3+}) ionic radius in $Cs_2NaLn(NO_2)_6$. Using the eigenvectors from the energy-level fit, the variation of the inverse magnetic susceptibility with temperature has been calculated between 1 and 100 K and the values are somewhat lower than those from experiment.

INTRODUCTION

The combination of 2-fold and 3-fold rotation axes, together with an inversion center, is not common for the point group symmetry of lanthanide ions (Ln^{3+}) in crystals. The T_h point group contains even (gerade, g) and odd (ungerade, u) symmetry representations of up to 3-fold degeneracy, as given in Table S1 of the Supporting Information. Some examples comprise praseodymium skutteridite (PrT_4X_{12}, where T = transition metal and X = pnictogen) compounds, such as $PrRu_4P_{12}$[1a] and $PrOs_4Sb_{12}$,[1b] which crystallize in the $Im\bar{3}$ space group, with the Pr^{3+} ion located at the center of an icosahedral cage of the 12 X atoms. The symmetry of the Ln^{3+} ion in the rare-earth double nitrates, such as $Pr_2Mg_3(NO_3)_{12}\cdot 24H_2O$,[2] is C_{3v}, but optical spectral analyses have been performed in T_h point group symmetry, with a slight distortion. Other examples comprise ML_6 systems, where ligand L has C_{2v} symmetry, such as H_2O and NO_2^-. The present study focuses upon the latter type, namely, in $Cs_2NaPr(NO_2)_6$, which has the face-centered-cubic structure (space group $Fm\bar{3}$) with four formula units per unit cell (Figure 1a). The Cs, Pr, and Na atoms are at fixed positions with T, T_h, and T_h point symmetries, respectively, where Pr^{3+} is 12-coordinated to oxygen. Some previous studies have investigated the structural,[3a] magnetic,[3b] and vibrational[3c] properties of this compound, and we have recently commented upon the electronic spectra of the corresponding Eu^{3+} complex.[3d,e] The structure of the Ln^{3+} complexes with the ligand NO_2^- differs from that of the transition metals, which are 6-coordinated to nitrogen in nitro complexes.[4] These systems have been extensively investigated, particularly with respect to their structures,[4a,b] phase transitions and Jahn−Teller distortions,[4c−h] and vibrational[4i−k] and electronic[4l−n] spectra.

The interpretation and modeling of the electronic spectra of Ln^{3+} in high-symmetry environments have fascinated us for a long time[5] because the minimum number of parameters is required for modeling of such systems,[5a,b] thus providing a stringent test for theory. Although recent progress has been made in ab initio methods in modeling of the energy levels of lanthanide ions,[6] the fitting error is much greater than that of crystal-field (CF) theory. A consistent interpretation and rationalization of the results from CF fittings of $4f^N$ energy levels has recently been made for lanthanide hexahaloelpasolites, Cs_2NaLnX_6 (X = Cl, F).[5b] Two CF parameters are required to fit the energy levels of Ln^{3+} in these LnX_6^{3-} complexes, and the fourth-order parameter B_0^4 is nearly an order of magnitude greater than the sixth-order parameter B_0^6 (using the Wybourne spherical tensorial notation throughout). The variation of B_0^4 across the

Received: June 8, 2011
Published: August 10, 2011

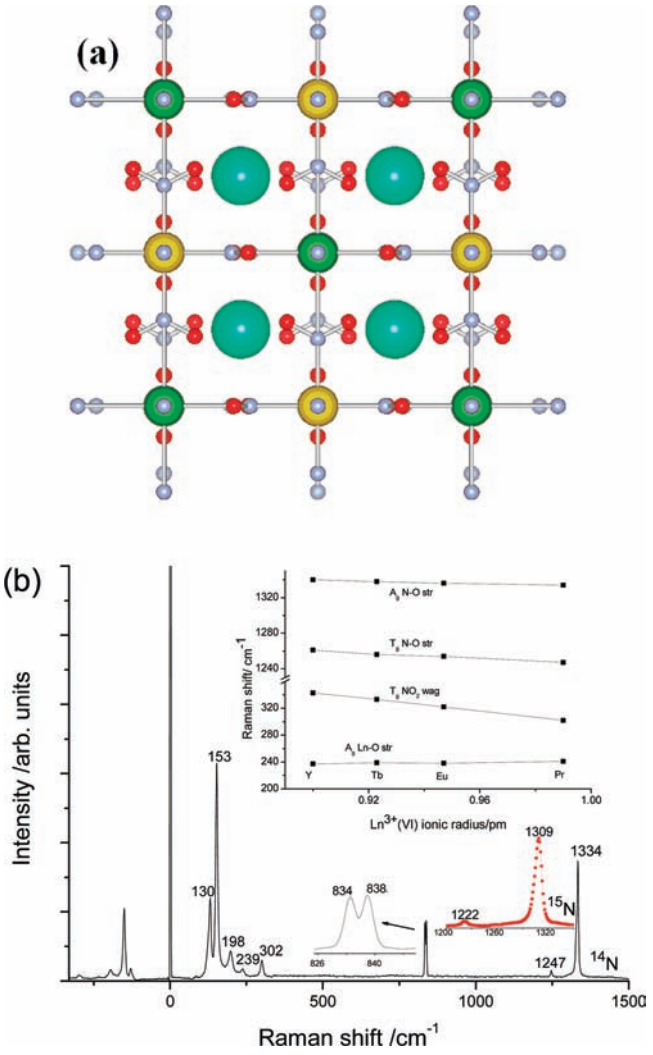

Figure 1. (a) Crystal structure of $Cs_2NaPr(NO_2)_6$ viewed in the direction along [100]. The large cyan balls are for Cs atoms at T sites, the intermediate green and yellow balls are for Na and Pr atoms at T_h sites, respectively, and the small red and gray balls are for O and N atoms at C_{2v} and C_s sites, respectively. (b) Fourier transform Raman spectrum of $Cs_2NaPr(NO_2)_6$. The region between 826 and 845 cm^{-1} is enlarged for clarity. The red (dashed) inset shows the stretching region of the ^{15}N-substituted compound. The inset plot shows the Raman shifts of several modes plotted against the Ln^{3+}(VI) ionic radii for Ln = Pr, Eu, Tb, and Y.

Ln^{3+} series was physically explained by a simple model involving the Ln^{3+}(VI) ionic radius and the 4f radial wave function.[5b] The fitting of the energy levels of Ln^{3+} can be further improved by including the configuration interaction of $4f^N$ with an equiparity configuration such as $4f^{N-1}np$.[5c] The energy-level scheme of the CF levels of Pr^{3+} is well-established in $Cs_2NaPrCl_6$,[5c] but we are unaware of previous systems where analyses have been performed for T_h site symmetry of this ion. The 12 oxygen ligands are responsible for the lowering of the symmetry and the existence of a further CF parameter, B_2^6.

There are only six irreducible representations (irreps) in the T_h molecular point group, labeled A, E, and T, with subscripts of g and u. All of the CF levels of $4f^2$ are labeled by g irreps, so that in the following the subscript is omitted. The T_1, T_2 and A_1, A_2 irreps of the O_h point group correlate with T and A (T_h), respectively. This makes the spectral selection rules less restrictive for the T_h point group than for O_h. Pure $4f^N-4f^N$ forced electric dipole (ED) transitions between electronic states are forbidden in T_h symmetry, so that the intensity of such transitions is restricted to the magnetic dipole (MD) or (much weaker) electric quadrupole mechanisms. The major intensity in the ED vibronic sidebands of transitions comprises odd-parity phonon modes. Tables showing the electronic and vibronic activities for various transitions are included in the Supporting Information (Tables S2 and S3). From magnetic measurements, Roser and Corruccini[3b] suggested that the irrep of the lowest CF level of the $^3H_4$ electronic ground state of Pr^{3+} in $Cs_2NaPr(NO_2)_6$ is either T or E. We find that the MD intensity ratios in the absorption spectra are only compatible with a T ($^3H_4$) ground state. This ground state is also confirmed by our CF calculations.

The electronic spectra of $Cs_2NaPr(NO_2)_6$ are much more complicated than those of $Cs_2NaPrCl_6$, and a detailed understanding was only achieved through knowledge of the vibrational behavior of this complex. The interpretation of the spectra is described in the following sections, together with the energy-level analysis. The results of the MD intensity and magnetic susceptibility calculations are also compared with the experiment.

EXPERIMENTAL SECTION

Crystals of the compositions $Cs_2NaPr(NO_2)_6$ and $Cs_2NaY(NO_2)_6$:Pr^{3+} (1 atom %) were synthesized by mixing a solution of the corresponding hexachloroelpasolites with a saturated solution of $NaNO_2$ at room temperature. The aqueous solutions were kept in the refrigerator for crystallization at about 4 °C. After a few days, transparent, yellowish crystals were obtained, which were removed from the mother liquor and dried. A sample of $Cs_2NaPr(^{15}NO_2)_6$ was prepared for Raman analysis by using $Na^{15}NO_2$. The hexachloroelpasolites were prepared by Morss method E[7] from CsCl (Strem), NaCl (Sigma-Aldrich), Y_2O_3 (International Laboratory USA), and Pr_6O_{11} (International Laboratory USA), all with nominal 99.999% purity. The $Cs_2NaLn(NO_2)_6$ (Ln = Y, Tb, Eu) complexes were analogously synthesized. Brooker and Irish[8] have pointed out the presence of nitrate impurities in nitrite complexes, and this was carefully checked.

IR Nujol mull and KBr disk spectra were recorded at room temperature in the range from 400 to 4000 cm^{-1} using a Nicolet FTIR instrument with resolution of 4 cm^{-1}. Raman spectra were recorded at room temperature by a Perkin-Elmer Spectrum 2000 spectrometer using a resolution of 4 cm^{-1}. The emission spectra were recorded at a resolution of 2–4 cm^{-1} by an Acton 0.5 m monochromator having a 1200 grooves mm^{-1} grating blazed at 500 nm, and a back-illuminated SpectruMM CCD detector, using an optical parametric oscillator (Panther) pumped by the third harmonic of a Surelite Nd:YAG pulsed laser. Near-IR and visible single-crystal absorption spectra were recorded by a Biorad FTS45A spectrometer using PbSe and photomultiplier tube detectors. The sample was housed in an Oxford Instruments closed-cycle cryostat or an Oxford Instruments Optistat CF continuous-flow top-loading static cryostat.

RESULTS AND DISCUSSION

Vibrational Analysis. The first-principles calculations were carried out using the density functional theory (DFT) plane-wave code VASP[9a] with the generalized gradient approximation (GGA) Perdew–Burke–Ernzerhof (PBE) exchange-correlation functional.[9b] The $5s^25p^66s^1$ electrons on Cs, the $2p^63s$ electrons on Na, the $5s^25p^64f^36s^2$ electrons on Pr, the $2s^22p^3$ electrons on N, and the $2s^22p^4$ electrons on O were treated as valence electrons in the calculations. The interaction between the valence

dx.doi.org/10.1021/ic201225k |Inorg. Chem. 2011, 50, 9004–9013

Table 1. Calculated (Columns 3 and 4) and Observed (Columns 5−7) Vibrational Frequencies (in cm^{-1}) for $Cs_2NaPr(NO_2)_6$[a]

		calculated		experimental		
irrep	type (major contribution)	4f-in-core	4f-in-valence	IR[3c]	Raman	vibronic
A_g	N−O sym str [ν_1 A_1 (C_{2v})]	1222	1330		1334s	1335
T_u	N−O antisym str	1211	1322	1335vw		1326−1332
E_g	N−O str	1209	1320			1263−1278
T_g	N−O str	1070	1251		1247w	1244−1249
T_u	N−O str [ν_3 B_2 (C_{2v})]	1049	1235	1220s		1233−1237
A_g	NO_2 sciss [ν_2 A_1 (C_{2v})]	787	820		838ms	846
E_g	NO_2 sciss	778	811		834ms	838−841
T_u	NO_2 sciss	774	809	830vs		827−833
T_u	NO_2 wag	387	310			291−307
T_g	NO_2 wag	384	306		302m	301
A_g	Pr−O sym str	285	235		239w	230−265
T_u	Pr−O antisym str	273	231	230s		217−244
T_g	NO_2 rock	252	207		198m	201−216
T_u	NO_2 rock	236	195	182		179−198
A_u	NO_2 twist	228	193			174−178
E_g	Pr-NO_2 str	208	184			
T_u	Pr-NO_2 str	200	165			156−171
T_g	NO_2 asym bend	185	149		153vs	158
T_u	Pr-NO_2 bend	169	131	140		145−152
T_g	Pr-NO_2 bend	143	129		130ms	131−138
E_u	NO_2 bend	136	115			121−127
T_u	Pr-NO_2 bend	109	101	100		100−113
T_g	Pr-NO_2 rot	79	73			66−90
T_u	Cs-PrNa(NO_2) trans	64	64	70		55−64
T_g	Cs trans	53	52			42−47
T_u	acoustic	2	2			

[a] The vibration types are str stretch, sym symmetric, antisym antisymmetric, sciss scissor, rot rotational, and trans translational. Intensities are qualitatively estimated by s (strong), m (medium), w (weak), v (very), and sh (shoulder). Refer to the text for explanations.

electrons and the core was described using the projected augmented wave method.[9c,d] The electron correlation associated with the Pr 4f electrons was treated by the GGA+U approach in which an effective on-site Coulomb repulsion with U_{eff} = 4 eV was added on Pr. Such a treatment was necessary to properly describe the spin state of Pr^{3+} with a spin moment of 2 μB. For comparison, calculations were also performed with the Pr 4f electrons treated as a part of the (chemically inert) inner core.

The N and O atoms in $Cs_2NaPr(NO_2)_6$ are located at sites with C_{2v} and C_s point symmetries, which depend on one and two internal parameters, respectively, with the calculated values being listed in Table S4 of the Supporting Information. As a first step in determining the vibrational frequencies, the internal parameters of the $Cs_2NaPr(NO_2)_6$ primitive cells were relaxed at the experimental lattice constant of 11.1728 Å[3b,c] until the total forces on each ion were less than 10^{-4} eV $Å^{-1}$. The Γ-point vibrational frequencies were then computed by a finite-difference approach with a step size of 0.02 Å. To ensure converged results, the cutoff energy for the plane-wave basis was set to 400 eV, the criterion for electronic minimization was 10^{-6} eV, and a 4 × 4 × 4 Monkhorst-Pack **k**-point grid (38 irreducible **k** points) was used to sample the Brillouin zone.

There are 66 vibrations of the $Cs_2NaPr(NO_2)_6$ crystal, some of which are doubly or triply degenerate. The $Pr(NO_2)_6^{3-}$ moiety modes transform as $3A_g + A_u + 3E_g + E_u + 5T_g + 8T_u$ (T_h). The description of the vibrational motions is included in Table 1 (column 2), and these basically fall into the categories of internal NO_2^- modes, Pr−ligand modes, and external (lattice) modes, although many vibrations are of mixed character. The assignment of bands in the IR and Raman spectra in Table 1 is based upon the selection rules that A_g, E_g, and T_g vibrations are Raman-active, whereas only T_u modes are IR-active.

The room temperature Raman spectrum of $Cs_2NaPr(NO_2)_6$ is shown in Figure 1b, and Raman shifts are given in column 6 of Table 1. The highest-energy vibrations correspond to N−O stretching (1247−1334 cm^{-1}) and N−O scissoring (834−838 cm^{-1}). The stretching modes shift to lower energy by 25 cm^{-1} in the ^{15}N-substituted compound, as shown in the figure. Additional data from the literature IR spectrum of Barnes and Peacock[3c] are given in column 5 with our new assignments (with some values omitted that may correspond to impurities). The range of vibrational frequencies derived from the low-temperature vibronic spectra (subsequently discussed) are also included in the Table 1 (column 7), and just as for $Cs_2NaPrCl_6$ vibronic spectra,[5c] multiple features may occur for each mode due to transverse-longitudinal mode splittings and the appearance of vibrations away from the zone center.

The NO_2 wagging mode of transition-metal hexanitro systems is at rather higher energy than herein: for example, at 623 cm^{-1} in $Na_3Co(NO_2)_6$.[4j] The N−O symmetric stretch [ν_1 A_1 C_{2v})] and

dx.doi.org/10.1021/ic201225k |Inorg. Chem. 2011, 50, 9004–9013

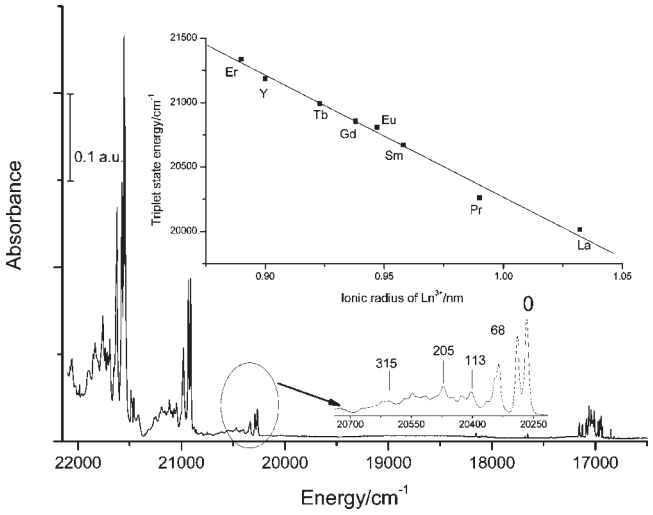

Figure 2. Survey 10 K absorption spectrum of $Cs_2NaPr(NO_2)_6$ between 22 100 and 18 450 cm^{-1}. The first group of NO_2^- triplet absorption bands is enlarged, with vibrational displacements from the first zero phonon line marked in cm^{-1}. The inset shows a plot of the triplet-state energy for $Cs_2NaLn(NO_2)_6$ (Ln = La, Sm. Er, Gd from ref 3f and Ln = Pr, Eu, Y, Tb from this work). The fitted line is $y = (29\,747 \pm 397) - (9481 \pm 418)x$; $R^2 = 0.9885$.

NO_2 scissor [ν_2 A_1 (C_{2v})] are located at 1326 ± 2 and 828 ± 3 cm^{-1} in $NaNO_2$.[10a,b] These values are fairly similar to the A_g (T_h) modes in $Cs_2NaPr(NO_2)_6$ (1334 and 838 cm^{-1}), showing that the bonding interaction of NO_2^- with its environment is mostly ionic. It has been pointed out that the trend in the bonding of the lower ligand molecular orbitals with the metal center can be followed from changes in the vibrational frequencies because a decrease in the metal−ligand bonding will lead to increased N−O frequencies and decreased metal−ligand frequencies.[11] The inset of Figure 1b, which compares the Raman shifts for $Cs_2NaLn(NO_2)_6$ (Ln = Pr, Eu, Tb, Y) as a function of the ionic radius of Ln^{3+}, shows that this is true for the NO_2 stretching and wag (and scissor, not shown) modes and the symmetric La−O stretch, although the change in the latter is only 1.7% from Ln = Pr to Y.

Using the optimized structure, the Γ-point vibrational frequencies for the $Cs_2NaPr(NO_2)_6$ primitive cell were computed and are included in the third and fourth columns of Table 1. The calculated 4f-in-valence frequency values >800 cm^{-1} (i.e., the NO_2 scissor, and stretch) are all larger than the corresponding 4f-in-core values, while for the lower frequency vibrations, the trend is reversed, except for the last two vibrations. The former trend is expected because the 4f bonding with the ligands is included in the 4f-in-valence calculations, but the latter trend is not readily explained. Certainly, however, the calculated 4f-in-valence frequencies are closer to experimental values.

The sensitivity of the vibrational frequencies was assessed in two ways (Table S5 of the Supporting Information). First, it was found that the calculated frequencies for the Pr^{3+} system were each slightly larger than the corresponding values of the La^{3+} system. This is expected from the comparison of the relevant lattice constants or ionic radii (compare with Figure 1b). Second, the effect of changing the cation from Cs^+ to Rb^+, with a lattice parameter decrease, was also investigated, and the calculated frequencies increased by a factor between 1% and 20% for the Rb^+ system.

Electronic Spectra of the NO_2^- Ion. Previous studies of the electronic spectra of the NO_2^- ion in $NaNO_2$ crystals,[10] and diluted $NaNO_2$ into alkali halides[12] have shown that the electronic ground state is the singlet $^1A_1$, with the lowest excited states corresponding to the triplet $^3B_1$ (18 959 cm^{-1} [10a]) and, at higher energy (25 980 cm^{-1} [10b]), the singlet $^1B_2$. The survey 10 K visible absorption spectrum of $Cs_2NaPr(NO_2)_6$ is shown in Figure 2. The weak $^3H_4 \rightarrow {}^1D_2$ absorption of Pr^{3+} is evident between 16 822 and 18 179 cm^{-1}, and at higher energy, commencing at 20 266 cm^{-1}, the $^1A_1 \rightarrow {}^3B_1$ transition of NO_2^- exhibits a strong progression in the frequency of 646 cm^{-1}. This vibration corresponds to the NO_2^- mode ν_2 A_1 (C_{2v}), which is a nearly pure bending mode. The marked reduction from its ground-state frequency of 838 cm^{-1} results from the electron transfer from a nitrogen nonbonding orbital to oxygen, so that the increased repulsion opens the O−N−O angle by ∼10°. Note the absence of strong progressions in ν_1, showing that the N−O bond distance is virtually unchanged in the excited state. The triplet-state energies show a marked increase for hexanitrito complexes with smaller lanthanide cations, obeying a linear relation with the Ln^{3+}(VI) ionic radius, as shown in the right-hand inset of Figure 2. The lower inset in Figure 2 shows the first group of bands in the NO_2^- triplet absorption spectrum in more detail, with some of the vibrational displacements from the 0−0 line marked, and the interpretation is analogous to the triplet spectrum of $NaNO_2$.[10a]

Emission Spectrum of Pr^{3+} in $Cs_2NaPr(NO_2)_6$. Several problems hinder the analysis of the electronic spectra of Pr^{3+} in $Pr(NO_2)_6^{3-}$. The first of these is that the lowest electronic state of NO_2^- is situated at 20 266 cm^{-1}, i.e., below the $^3P_0$ level of Pr^{3+}, which is calculated to be at ∼20 900 cm^{-1}. Thus, the emission from $^3P_0$ is quenched, and the observation of $^3P_0$ and higher energy levels of Pr^{3+} is difficult. This severely limits the experimental information content concerning Pr^{3+} energy levels.

Excitation into NO_2^- absorption bands leads to Pr^{3+} emission in $Cs_2NaPr(NO_2)_6$, as shown in Figure 3a for the highest-energy group of bands in the 10 K emission spectrum of $Cs_2NaPr(NO_2)_6$, corresponding to the $^1D_2 \rightarrow {}^3H_4$ transition. This spectrum enabled the assignment of the $^3H_4$ CF levels, with the vibronic sidebands being strongest for the first two transitions to the T and E CF levels of $^3H_4$. The locations of the 0−0 transitions are indicated in the figure. The observed vibronic structure is summarized in Table 2 for each transition. Here, and subsequently, values given in parentheses denote that more than one assignment is possible for a given band so that only one, or more, of the alternative assignments may be applicable. Several weak bands are observed below 14 474 cm^{-1}, corresponding to $^1D_2 \rightarrow {}^3H_5$, but firm assignments cannot be made.

We aimed to further explore the energy-level system of Pr^{3+} in hexanitrito complexes by dilution of Pr^{3+} into another hexanitrito host lattice. Unfortunately, we were unable to observe the emission of Pr^{3+} in samples of $Cs_2NaY(NO_2)_6$:Pr^{3+} because of the presence of a strong NO_2^- emission and also of a Eu^{3+} impurity emission. The survey emission spectra of $Cs_2NaY(NO_2)_6$:Pr^{3+} (1 atom %) between 22 000 and 14 200 cm^{-1} are shown in Figure 3b at three different temperatures. The ν_2 NO_2^- progression in 849 cm^{-1} exhibits a maximum intensity at the third member, $\nu_2 = 3$. With increasing temperature, however, the $^5D_0 \rightarrow {}^7F_1$ transition of the trace impurity Eu^{3+} [3d] dominates the entire spectrum. The inset shows an activation energy plot, and from the slope ($-E_a/R$), an energy of 19 cm^{-1} is indicated. Presumably, this is the energy barrier for transfer from the NO_2^- triplet state to the lowest CF level of $^5D_2$ Eu^{3+}, which is then estimated to be at ∼21 300 cm^{-1}. The fact that this transfer does

dx.doi.org/10.1021/ic201225k |Inorg. Chem. 2011, 50, 9004–9013

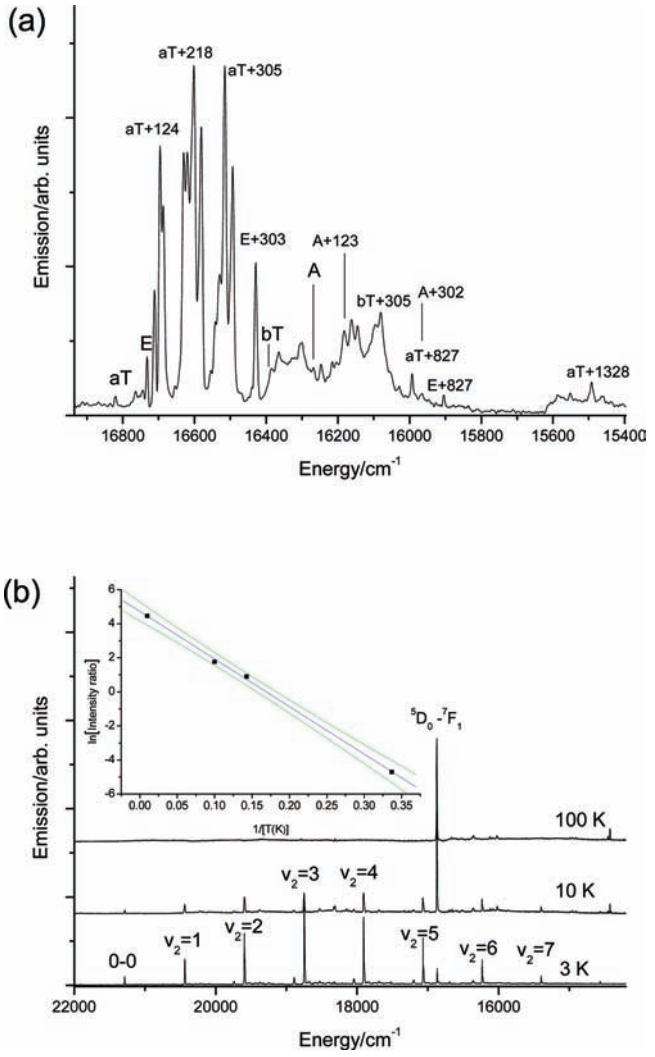

Figure 3. (a) 450 nm excited emission spectrum of $Cs_2NaPr(NO_2)_6$ between 16 920 and 15 400 cm^{-1} at 7 K. (b) 430 nm excited emission spectrum of $Cs_2NaY(NO_2)_6$:Pr^{3+} (1 atom %) between 22 000 and 14 200 cm^{-1} at 3, 10, and 100 K. The members of the progression in the NO_2 scissor mode, as well as the $^5D_0 \rightarrow {}^7F_1$ transition of Eu^{3+}, are marked. The inset shows an activation energy plot of the natural logarithm of the intensity ratio of the $\nu_2 = 3$ band and the $^5D_0 \rightarrow {}^7F_1$ band versus reciprocal temperature for T = 3, 7, 10, and 100 K. The graph is fitted by $y = (4.7 \pm 0.1) - (27.9 \pm 0.7)x$; $R^2 = 0.999$. The 95% confidence limits are shown.

not involve Pr^{3+} is exemplified by the same occurrence for some other Ln^{3+} diluted into $Cs_2NaY(NO_2)_6$.

IR Electronic Absorption Spectra of Pr^{3+} in $Cs_2NaPr(NO_2)_6$. The 10 K IR and visible absorption spectra of Pr^{3+} in $Cs_2NaPr(NO_2)_6$ are shown in detail in Figure 4, and band assignments *for all features* are collected in Table 2. With the exception of a few hot bands in Figure 4c, all of the transitions originate from $^3H_4$ aT and the terminal states and associated vibronic energies are marked in the figure for selected bands. Table S2 of the Supporting Information shows that transitions from the electronic ground state $^3H_4$ T are potentially MD-allowed to all upper states. However, because of SLJ selection rules, most of the transitions are very weak. The strongest MD transition in the IR absorption spectrum is at 4404 cm^{-1}, and using this intensity as a reference for comparison, the calculated and measured relative intensities of other MD transitions from $^3H_4$ T are listed in Table 3. Measurements of the IR absorption spectrum were also made at 60 K because only T upper states will exhibit the 89 cm^{-1} hot band from $^3H_4$ A. In fact, in most cases, the hot band was too weak to be observed, with the exception of transitions to $^3H_6$ aT and $^3F_3$ aT. The $^3H_4 \rightarrow {}^3H_6$ transitions are observed above 3950 cm^{-1} and comprise some sharp MD zero phonon lines and associated vibronic sidebands (Table 2 and Figure 4a). The zero phonon lines of the two $^3H_4$ T $\rightarrow {}^3F_2$ transitions are readily assigned at 5359 and 5396 cm^{-1}, with extensive vibronic structure to higher energy (Figure 4b), which is partly overlapped by the NO_2^- stretching modes of the $^3H_4$ T $\rightarrow {}^3H_6$ transitions. The aT and A CF levels of $^3F_3$ are assigned from the zero phonon lines at 6556 and 6565 cm^{-1}, with a measured (calculated) intensity ratio of 7:1 (7:1). The vibronic structure is assigned to the low energy of each origin (Table 2). The spectrum is complex up to 8480 cm^{-1}, but the NO_2^- modes were invaluable in making assignments for the remaining $^3F_3$ and $^3F_4$ CF levels (Figure 4d). The only unassigned bands are some very weak features between 7472 and 6786 cm^{-1}, which could otherwise be assigned to first members of the progression in the A_g Pr−O symmetric stretching mode.

Near-IR and Visible Absorption of Pr^{3+} in $Cs_2NaPr(NO_2)_6$. The $^3H_4 \rightarrow {}^1G_4$ spectrum (Figure 4e) is relatively uncluttered and well-resolved, so that it serves as a model fingerprint for the lower-energy vibronic sideband. The MD intensities from $^3H_4$ aT are calculated in the ratio of 1.00 T:0.23 A:0.60 aE:0.24 bE, and those observed are 1.00:(0.2):1.1:0.3. The lowest-energy transition (to T) is heralded by a strong zero phonon line, and it is the only one that exhibits the 89 cm^{-1} hot band at higher temperatures. The next transition (to A) exhibits a very weak vibronic sideband. We note that the T $\rightarrow$ T + 305 cm^{-1} band is split by ~4 cm^{-1}, so that the assignment of one component to the 0−0 band of T $\rightarrow$ A accounts for the two very weak (but strongest) features to high energy as the 123 and 188 cm^{-1} vibronic origins. The next origin (at 10 164 cm^{-1}) is also marked by a relatively strong MD origin, as is the T $\rightarrow$ E transition at 10 418 cm^{-1}.

The lowest-energy zero phonon line of the $^3H_4$ T $\rightarrow$ E $^1D_2$ transition (Figure 4f) is coincident with that in the emission spectrum. There are sharp bands at 27 cm^{-1} to the high energy of the 0−0 line, as well as at this interval to the high energy of the vibronic structure (Figures 4f,g). The origin of these features requires further study. The vibronic structure of $^3H_4$ T $\rightarrow$ T $^1D_2$ is very weak. As mentioned above, the higher energy absorption bands of Pr^{3+} in $Cs_2NaPr(NO_2)_6$ are buried in the NO_2^- triplet absorption bands. One tentative assignment can be given for $^3H_4$ T $\rightarrow$ T $^3P_1$ to a new, sharp band at 21 531 cm^{-1}, which is not repeated in the 646 cm^{-1} progression, but this has not been included in the CF analysis.

CF Analysis. The first 20 (degeneracy 45) of the 25 energy levels (degeneracy 56) experimentally identified as belonging to the ^3H_J (J = 4, 6), ^3F_J (J = 2−4), $^1G_4$, and $^1D_2$ multiplets of the $4f^2$ electronic configuration (degeneracy 91) of the Pr^{3+} ion in $Cs_2NaPr(NO_2)_6$ were fitted to the standard Hamiltonian.[5c] In view of the restricted number of assigned levels, only a few of the adjustable free ion parameters were varied in the energy-level fitting, namely, the Slater parameters F^k (k = 2, 4, 6) and the spin−orbit coupling constant, $\zeta(4f)$. The values of the configuration interaction parameters α, β, and γ, as well as of the $k = 0$ magnetic interaction parameter M^k ($M^2 = 0.56M^0$; $M^4 = 0.38M^2$), were held constant and equal to those of the elpasolite compound $Cs_2Na\,PrCl_6$.[5c]

dx.doi.org/10.1021/ic201225k |*Inorg. Chem.* 2011, 50, 9004–9013

Table 2. Assignment of Vibronic Structures in the Spectra of $Cs_2NaPr(NO_2)_6$[a]

transition	0−0 energy (cm^{-1})[b]	vibronic structure (cm^{-1})
		Absorption from $^3H_4$ aT to
aA H_6	*3950*	110vw, 125w, 190vw, 226vw, 240vw, 305vw, 830w
aT H_6	*4312*	55vw, 76w, 102sh, 111w, 123sh, 134m, (150vw), (170mw), 182vw, (192vw), (203m), 211sh, 220sh, (226sh), (241mw), (294w), 302w, 828mw, (1235m), (1246w), (1270m), (1326mw)
bT H_6	*4404*	(58vw), (78mw), (100vw), (111m), 123m, 134w, (149mw), 158vw, (174m), 188mw, (202w), 215vw, 219mw, (231sh), (257mw), 303mw, (1235mw), 1246w, 1271w, 1330mw
E H_6	*4579*	(56sh), (82mw), 109mw, 124mw, 134mw, (152w), 167sh, 178mw, (189w), (219m), (240ms), (262sh), (303ms), 1235w, 1263sh, 1276w, 1330vw
cT H_6	4696	(72w), (102m), (123ms), 133sh, (145sh), (171sh), (186ms), 190sh, 202mw, (228s), (244m), 303mw, (832m), 1236mw, 1248w, (1269mw), 1331mw
bA H_6	4729	(100w), (112sh), 134m, (169w), (195s), (211m), 217sh, 227sh, 240sh, 302mw, (832w), (1236mw), 1270w, 1330mw
T $^3F_2$	*5359*	58vw, 109m, 113sh, 122m, 132w, 136w, 158w, 181mw, (188ms), (202w), 211sh, (223s), 234sh, (240m), 305m, 831mw, 841vw, (1235mw), (1246w), (1271m), (1332ms)
E $^3F_2$	*5396*	107m, 110sh, 126sh, (132m), 181sh, (186s), (203m), 217w, 229w, 301mw, 828mw, 838vw, 846vw, (1235mw), (1246w), 1330w
aT $^3F_3$	*6556*	(41mw), (56w), (74mw), 88mw, 108s, 111sh, 121s, (135s), (159vw), 182s, 187s, 201m, 212sh, 219m, 231ms, 240ms, 302s, 829s, 1234ms, 1246mw, 1271m, 1330m, (1335sh)
A $^3F_3$	*6565*	(42w), 111s, 121sh, 305vw, 831sh, 1269sh, (1326sh)
bT $^3F_3$	*6705*	109m, 122 ms, 133mw, 181sh, 187vs, 202vw, 198w, 210vw, 219w, 232vw, 241m, (252vw), 302m, 828mw, (1235m), 1249sh, (1271ms), 1278sh, 1330mw
aT $^3F_4$	*6931*	(26vw), 47mw, 57vw, 127w, 135w, 157w, 190sh, 203mw, 222m, 234sh, 241m, (253sh), 304w, 829mw, 1235w, 1248vw, 1271w, 1330w
A $^3F_4$	*7100*	(84sh), 103m, (124m), 134mw, (158w), (179m), (191sh), (218sh), (235ms), (251sh), 305w, 832mw, 1237w, (1248sh), 1273vw, 1332vw
E $^3F_4$	7112	(112m), (122mw), (157sh), (179sh), (206sh), (239sh), (828m), (1236sh), (1271w)
bT $^3F_4$	7148	(110w), (121sh), (131m), (187ms), (203sh), 219m, 232sh, 301mw, 305mw, (828m), (1236w), 1244sh, 1270vw, 1330w
T $^1G_4$	*9619*	43vw, 56vw, 77vw, 109m, 123m, 135mw, 149m, 158vw, 184s, 188ms, 201w, 213mw, 219m, 230mw, 238m, 291vw, 305m, 829mw
A $^1G_4$	9918	44vw, 55vw, 74vw, 87vw, 104vw, 123w, 156vw, 188w, 224vw, 240sh
aE $^1G_4$	*10 164*	44vw, 122m, 132vw, 176sh, 181mw, 188mw, 202vw, 218w, 231mw, 239mw, 305vw, 828vw
bE $^1G_4$	*10 418*	25vw, 39vw, 46vw, 100sh, 106m, 121m, 133mw, 175sh, 187ms, 200mw, 211sh, 218mw, 232mw, 239m, 263vw, 275vw, 294w, 302m
E $^1D_2$	*16 822*	(27m), 45vw, 70vw, 79vw, 98vw, 108m, 111m, 124ms, 135ms, 179vw, 188s, 202mw, 219s, 231m, 240s, 307ms, 830m, 1235mw, 1248w, 1271mw, 1331m
T $^1D_2$	*17 126*	66w, 90vw, 107w, 132w, 159w, 186w, 221w, 305w
		Absorption of NO_2^-
$^1A_1 \rightarrow {}^3B_1$	*20 266*	(23ms), 68m, 79sh, 100vw, 136w, (160w), (181w), (202mw), (250w), 283w, 301w, 644s
		Emission from $^1D_2$ E to
A $^3H_4$	*16 267*	(64vw), (85m), (121mw), 134w, 157vw, (187m), 202sh, 216w, 238w, 302w, (830vw)
bT $^3H_4$	*16 385*	49vw, 56w, 66w, 78w, 85w, 95sh, 106vw, 138w, (156vw), 182w, 203m, 223m, (239m), (288mw), 305m, 833w
E $^3H_4$	*16 732*	(121ms), (177w), (189w), (217s), 231sh, 239ms, 292vw, 303ms, 827mw, 1273w, 1327vw
aT $^3H_4$	*16 822*	32vw, 44vw, 56w, 65vw, 76w, 109m, 124s, 133ms, 178sh, (190ms), 200m, (212sh), 218s, 239ms, (265w), (289w), 305s, 827mw, 1233mw, 1248w, (1268mw), 1328m

[a] Intensities are qualitatively estimated by s (strong), m (medium), w (weak), v (very), and sh (shoulder). [b] Observed zero phonon lines are in italics.

dx.doi.org/10.1021/ic201225k |*Inorg. Chem.* 2011, 50, 9004–9013

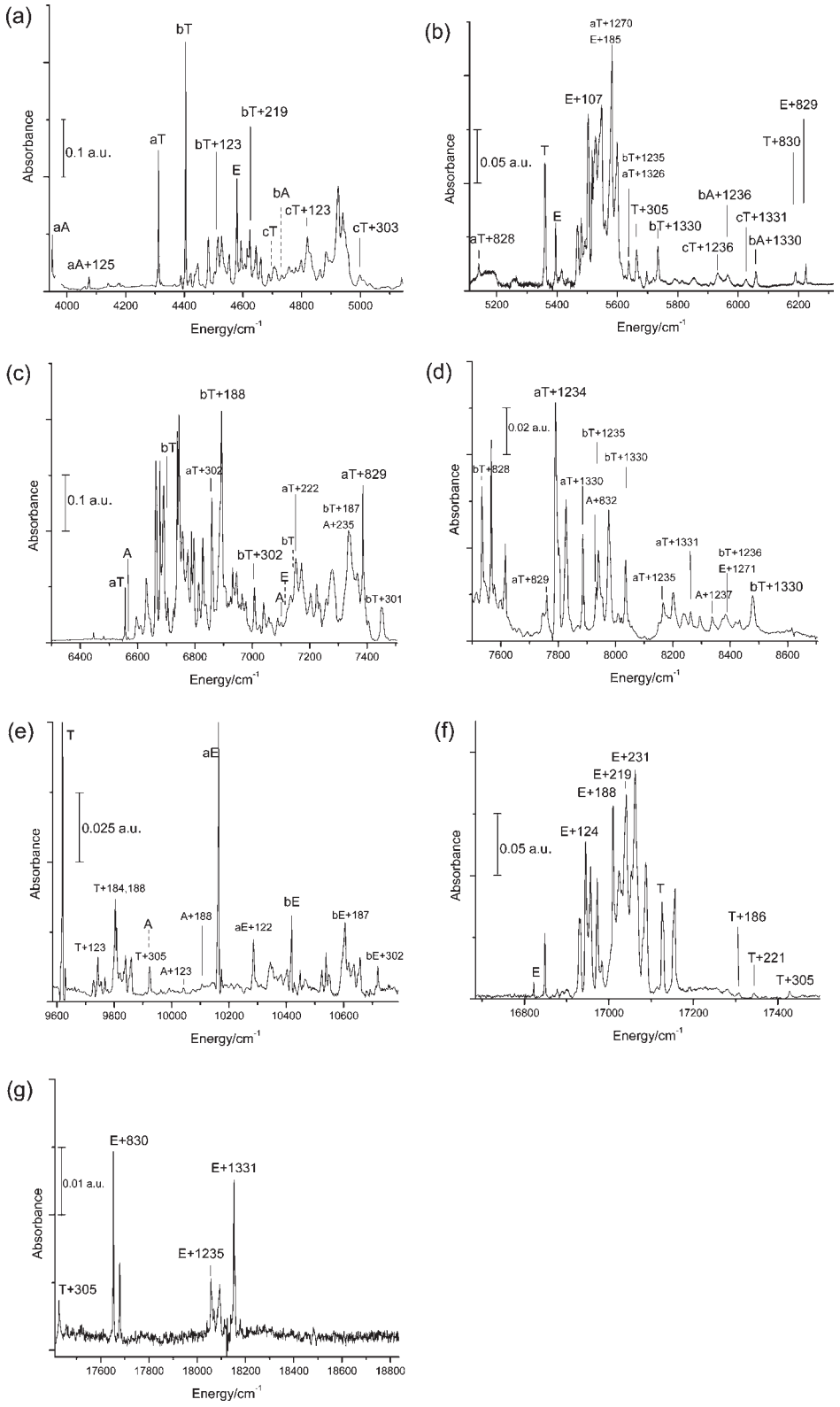

Figure 4. 10 K absorption spectra of $Cs_2NaPr(NO_2)_6$ between 3940 and 18 800 cm^{-1}. The initial state is $^3H_4$ aT. Zero phonon lines are indicated by full (dashed) lines if observed (inferred), and some terminal vibronic levels are indicated by the respective vibrational energies: (a) 3940−5145 cm^{-1}; (b) 5110−6315 cm^{-1}; (c) 6300−7505 cm^{-1}; (d) 7500−8705 cm^{-1}; (e) 9585−10 790 cm^{-1}; (f) 16 700−17 500 cm^{-1}; (g) 17 400−18 800 cm^{-1}. Note the changes in the absorbance scale.

The tetrahedral point group symmetry imposes three independent CF parameters: B_0^4, B_0^6, and B_2^6. The parameters B_0^4 and B_4^4 are constrained by the cubic ratio $B_4^4 = \pm B_0^4(5/14)^{1/2}$ and $B_4^6 = \mp B_0^6(7/2)^{1/2}$, while $B_6^6 = -B_2^6(5/11)^{1/2}$. The choice of the B_2^6 sign

dx.doi.org/10.1021/ic201225k |*Inorg. Chem.* 2011, 50, 9004–9013

is arbitrary, and it has no influence on the energies of the levels. Hence, the total number of parameters thus far is equal to 7.

The point charge model and the covaloelectrostatic model[13a,b] were utilized to obtain starting values of the CF parameters. The calculations relied on the crystal structure of the $Cs_2NaLn(NO_2)_6$ compounds (Table 4). The structure of the lanthanum compound[3c] was utilized to calculate the CF parameters of $Cs_2NaPr(NO_2)_6$. The edge of the cubic cell measures 11.38 Å. The sums were performed over the 18 nearest ions, i.e., 12 O atoms at 2.823 Å and 6 N atoms at 3.186 Å. The parameters were evaluated in the following situations: (i) O alone with a charge of 1−; (ii) O and N bearing nominal ionic charges of 2− and 3+, respectively; (iii) NO_2^- charges given by molecular orbital calculations: −0.422 on O1 and O2; −0.156 on N. It has been empirically found[13a] that, for neodymium compounds, the fourth- and sixth-order point charge contributions give realistic values when multiplied by factors approximately equal to 2.2 and 6.8, respectively. The resulting values for the CF parameter under the various scenarios above are reported in Table 4, lines 3−5.

In the covaloelectrostatic model, the predicted parameters contain a fraction of the point charge contribution added to a part due to kinetic energy interaction. Two hypotheses were retained: (i) the interaction occurs independently between the central ion Pr and its O and N ligands; (ii) the interaction occurs between O and N in addition. The resulting calculated values for the CF parameter are listed in Table 4, lines 7 and 8. The indications of this table are far from conclusive for the values of the CF parameter. It seems probable that B_0^6 is negative and that its absolute value is smaller than that of B_2^6. As for B_0^4, there is no concordance: neither for the sign nor for the magnitude. The parameter might be located between −384 and 856 cm^{-1}.

Therefore, a series of fittings within and without the range of possible parameter values was undertaken, looking for the best match between experimental and calculated energies. The seven parameter values for a fitting with a mean deviation of 33 cm^{-1} are listed in Table 5, with a comparison of the experimental and calculated CF level energies given in Table 3. The resulting ratios F^2/F^4 and F^4/F^6 are 1.36 and 1.56, respectively, and are fairly close to those for the $Cs_2NaLnCl_6$ series and to those expected for a Coulomb field. An improvement of the fit occurred by adding the electrostatically correlated spin−orbit interaction P^k parameter ($k = 2$ with $k = 4, 6$ restricted by $P^4 = 0.75P^2$ and $P^6 = 0.5P^2$), which allows for the effect of additional configurations upon the spin−orbit interaction, to the list of adjustable parameters, so that in total, eight parameters were employed in the energy-level fitting (CFIT_2, Table S6 of the Supporting Information). Further parameter variations (CFIT_3,4, Table S6 of the Supporting Information) did not lead to fitting improvements, but the final configuration interaction (α, β, γ) and magnetic (M^0: with M^2 and M^4 restricted as given above) parameter values were reasonably similar to those for $Cs_2NaPrCl_6$.

MD absorption intensities were calculated as described in the Supporting Information utilizing the eigenvectors determined in the previous step, and the values have been compared with the experimental integrated intensities in columns 6 and 7 of Table 2. The agreement for the $^3H_4$ T → $^3H_6$ transitions is satisfying and seems to prove the correctness of the assignments. However, the agreement deteriorates for higher energies.

The magnetic susceptibility of $Cs_2NaPr(NO_2)_6$ between 1 and 100 K was calculated by Van Vleck's formula (given in the Supporting Information),[13c,d] using the previously determined eigenvectors. The variation of $1/\chi$ with the temperature is shown in Figure 5 and compared with the experimental results of Roser and Corruccini.[3b] Our calculated value at 100 K is only 63% that

Table 3. Experimental and Calculated Energies of Pr^{3+} in $Cs_2NaPr(NO_2)_6$ and MD Absorption Intensity Ratios

					integrated MD absorption intensity ratio for transitions from $^3H_4$ T	
$^{2S+1}L_J$	irrep[a]	exptl[b]	calcd[c]	calcd − exptl	calcd: $100I/I_{4404}$	exptl: $100I/I_{4404}$
$^3H_4$	aT	0	0	0		
	E	89	112	23		
	bT	437	461	24		
	A	555	556	1		
$^3H_5$	aT		2118			
	E		2289			
	bT		2417			
	cT		2518			
$^3H_6$	aA	3950	3928	−22	6	10
	aT	4312	4272	−40	12	56
	bT	4404	4446	42	100	100
	E	4579	4579	0	79	82
	cT	4696	4689	−7	17	<10[d]
	bA	4729	4705	−24	27	<4[d]
$^3F_2$	T	5359	5308	−51	33	65
	E	5396	5393	−3	29	22
$^3F_3$	aT	6556	6593	37	98	26
	A	6565	6595	30	8	4
	bT	6705	6679	−26	83	29
$^3F_4$	aT	6931	6907	−24	6	28
	A	7100	7113	13	18	12
	E	7112	7113	1	15	[d]
	bT	7148	7144	−4	35	[d]
$^1G_4$	T	9619	9666	47	25	34
	A	9918	9997	79	6	[d]
	aE	10 164	10 292	128	15	38
	bE	10 418	10 374	−44	6	10
$^1D_2$	E	16 822	16 787	−35	4	3
	T	17 126	17 043	−83		
$^3P_0$	A		20 892			
$^3P_1$	T		21 497			
$^1I_6$	aT		21 644			
	E		21 696			
	aA		21 710			
	bT		21 934			
	cT		22 032			
	bA		22 120			
$^3P_2$	E		22 677			
	T		22 714			
$^1S_0$	A		46 657			

[a] Irrep: irreducible representation. [b] Exptl: experimentally determined energy level. [c] Calcd: calculated energy level using seven adjustable parameters (Table 5, column 2; Table S6 of the Supporting Information, CFIT_1) for the first 20 levels determined (i.e., up to $^1G_4$ T). [d] Intensity estimations for these transitions are unreliable because either the transition is not observed or it is buried in the vibronic structure.

dx.doi.org/10.1021/ic201225k |Inorg. Chem. 2011, 50, 9004–9013

Table 4. Starting Values of the CF Parameters of $Cs_2NaPr(NO_2)_6$ Given by the Point Charge Model and the Covaloelectrostatic Model Utilizing the Structural Data[13b] for $Cs_2NaLa(NO_2)_6$: La (4a) (0, 0, 0), O (48h) (0, 0.100, 0.227), and N (24e) (0, 0, 0.280)[a]

point charges				
oxygen	nitrogen	B_0^4	B_0^6	B_2^6
−1	0	683	−63	−383
−2	+3	−384	−221	−769
−0.422	−0.156	380	22	−162
covaloelectrostatic				
interaction Pr−N−O		−300	−235	−674
interaction Pr−O Pr−N		856	3	−674

[a] According to ref 13a, the multiplying factors in the point charge model are equal to 2.063 and 6.837 for the fourth- and sixth-order CF parameters, respectively. Tabulated values are in cm^{-1}.

Table 5. Empirical Hamiltonian Parameters (in cm^{-1}) of Pr^{3+} in $Cs_2NaPr(NO_2)_6$ and $Cs_2NaPrCl_6$ and Fitting Results

parameter	$Cs_2NaPr(NO_2)_6$ ($4f^2$) with T_h[a]	$Cs_2NaPrCl_6$ $(4f^2)^{5c}$ with O_h	$Cs_2NaPrCl_6$ $(4f6p)^{5c}$ with O_h
F^2	68 955	67 647	67 499
F^4	50 729	48 950	48 274
F^6	32 592	31 963	31 222
α	[23.50]	23.5	22.9
β	[-690]	−690	−698
γ	[1684]	[1684]	[2035]
M^0	[2.36]	2.36	3.33
P^2			
ζ(4f)	747.8	752.5	756.1
B_0^4(f,f)	−875	1996	3435
B_0^6(f,f)	−470	222	606
B_2^6(f,f)	−1563		
B_0^4(f,p)			28 900
X^2(f,f,f,p)			1.32
X^4(f,f,f,p)			1.46
fitting data[b]			
N	20	38	38
n_p	7	10	13
δ	33.0	32.7	11.6

[a] Parameters in square brackets were held fixed in the energy-level fits. [b] N = number of levels; n_p = number of parameters; δ = mean deviation, cm^{-1}.

reported,[3b] and it is close to the straight line representing the Curie law for the free-ion $^3H_4$ ground state. The calculated curve starts more steeply at low temperatures than the free-ion line and then becomes almost parallel above it. Modifying the CF parameters did not result in an increase of $1/\chi$ sufficient to match the experimental values. A number of CF parameter sets (however, unrealistic because they gave no match of the electronic energy levels) were tried, but none could lead to a value as high as 130 mol cm^{-3} at 100 K. The calculated values would agree with a compound where only $^2/_3$ of the rare-earth sites were occupied, which is in contradiction with the crystallographic determination.[3b,c] According to the CF calculation, the $^3H_4$ levels sufficiently populated to intervene

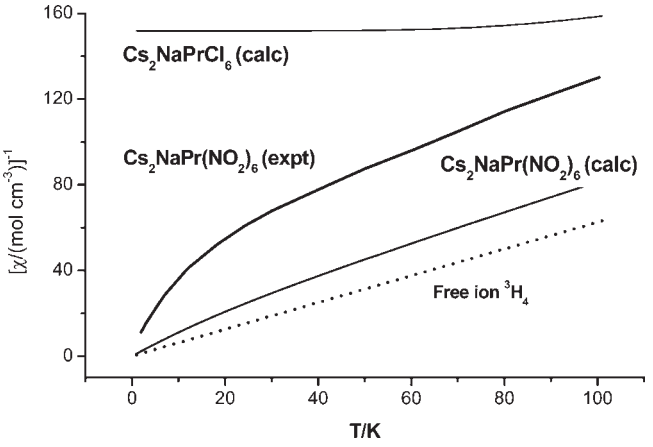

Figure 5. Calculated reciprocal molar magnetic susceptibility of $Cs_2NaPr(NO_2)_6$ and comparison with the experimental value, that of $Cs_2NaPrCl_6$, and the $^3H_4$ free-ion value.

in the calculation of the magnetic susceptibility are the T ground state and the E level. The two remaining $^3H_4$ levels are located at much higher energies. It is noted that Roser and Corrucini pointed out that $Cs_2NaPr(NO_2)_6$ has the most unusual susceptibility of any compound in the series.[3b]

The calculated reciprocal molar susceptibility of the elpasolite $Cs_2NaPrCl_6$ is also shown in Figure 5, and it displays a nearly constant value of $1/\chi$ approximately equal to 150 mol cm^{-3} in the same temperature range. In this system, the lowest calculated levels of $^3H_4$ follow the sequence: A, T_1, E, and T_2 at 0, 219, 370, and 645 cm^{-1}.[5c] The reason for the plateau between 0 and 100 K is the wide gap between the A ground-state level and the first triply degenerate level T_1.

Such high deviations in the calculations of electronic properties are not unusual in the case of Pr^{3+}. For instance, the mean deviation of the energy-level fit for $Cs_2NaPrCl_6$ was equal to 32.7 cm^{-1} when the calculation was carried out in the $4f^2$ basis alone. However, the inclusion of the configuration interaction with p ligand electrons brought the deviation down to 11.6 cm^{-1}.[5c] This interaction requires large fourth-order CF parameters because they are the only ones likely to act between f and p electrons because k (even) has to be comprised between $l_f - l_p$ and $l_f + l_p$. The unique possibility is $k = 4$ because the second-order parameters are null in the T_h point group. In the case of the elpasolite $Cs_2NaPrCl_6$, B_0^4 is 10 times larger than B_0^6 (Table 5) and this makes it an ideal candidate for configuration interaction. It is not the case herein, where the fourth-order parameters are smaller than the sixth-order ones. Besides, even if it were not so, the number of experimental energy levels is too small to afford two or three more parameters. The major discrepancies in the experimental−calculated energies listed in Table 3 (column 5) are for the unambiguously determined T level at 4404 cm^{-1}, the two highest $^1G_4$ levels at 10 164 and 10 418 cm^{-1}, and the $^1D_2$ levels at 16 822 and 17 126 cm^{-1}. There exists probably a missing contribution, presently unexplained, that touches the CF interaction but also probably the free-ion parameters because, if the parameter P^2 is omitted, the mean deviation climbs up.

■ CONCLUSIONS

Major differences arise in the electronic spectra of the elpasolites $Cs_2NaPr(NO_2)_6$ and $Cs_2NaPrCl_6$, partly because the electronic ground state is triply degenerate in the first case and singly

dx.doi.org/10.1021/ic201225k |Inorg. Chem. 2011, 50, 9004–9013

degenerate in the second. Furthermore, the spectra of $Cs_2NaPr(NO_2)_6$ are considerably more complex because of the presence of two-center transitions, and there is a cutoff in the Pr^{3+} information content above ~20 000 cm^{-1}, although two-photon experiments could prove to be useful in this respect. The firm knowledge of the vibrational assignments for $Cs_2NaPr(NO_2)_6$ was essential for understanding the complex electronic spectra. In particular, the fingerprints of the accurately known frequencies of the NO_2^- scissor (830 cm^{-1}) and NO_2^- stretching modes (1235−1330 cm^{-1}), which are displaced far from the zero phonon lines of transitions, were invaluable in assigning or confirming the 0−0 transition energy. The energy level and MD intensity calculations also proved important for making assignments.

Some of the problems in the analyses have been highlighted. Notably, there is an unaccounted-for interaction, presumably related to the nitrito ligand, that leads to poor predictions of some $4f^2$ CF energy levels. Second, the magnetic susceptibility shows an unexplained behavior, and a new experimental determination would be useful in this respect. Overall, however, there has been success in accounting for the complex vibrational and electronic spectra of Pr^{3+} in $Cs_2NaPr(NO_2)_6$. The most striking findings are the weak fourth-order CF of Pr^{3+} and the almost exclusive electrostatic interaction with the NO_2^- ligand.

■ ASSOCIATED CONTENT

Ⓢ Supporting Information. Group theoretical tables, calculated vibrational frequencies, calculated internal parameters, empirical Hamiltonian parameters, experimental and calculated energies, the van Vleck formula, and calculation of the MD oscillator strengths (Tables S1−S7). This material is available free of charge via the Internet at http://pubs.acs.org.

■ AUTHOR INFORMATION

Corresponding Author
*E-mail: bhtan@cityu.edu.hk.

Notes
[§]Deceased.

■ ACKNOWLEDGMENT

We thank Dr. C. S. K. Mak for contributions during the early part of this study. M.D.F. was indebted to Dr. E. Soulié (DRECAM, CEA Saclay) for a stimulating discussion and for providing documents. Financial support from the Hong Kong UGC GRF fund CityU 102609 (to P.A.T.) and the National Science Foundation of China (Grant 10804001 to L.N.) is gratefully acknowledged.

■ DEDICATION

In Memoriam: Michèle Faucher passed away on May 7, 2011, near the end of this work. It was with great sadness that we completed the manuscript, and we dedicate this work to her memory. She was an outstanding and prolific researcher in the physics and chemistry of lanthanide-ion systems and will be severely missed by the research community.

■ REFERENCES

(1) (a) Aoki, Y.; Namiki, T.; Matsuda, T. D.; Abe, K.; Sugawara, H.; Sato, H. *Phys. Rev. B* **2002**, *65*, 644461–644467. (b) Tayama, T.; Sakakibara, T.; Sugawara, H.; Aoki, Y.; Sato, H. *J. Phys. Soc. Jpn.* **2003**, *72*, 1516–1522.

(2) Devine, S. D. *J. Chem. Phys.* **1967**, *47*, 1844–1852.

(3) (a) Barnes, J. C.; Al-Rasoul, K.; Harkins, P. *J. Chem. Soc. Pak.* **1980**, *2*, 9–14. (b) Roser, M. R.; Corruccini, L. R. *Phys. Rev. B* **1990**, *41*, 2359–2368. (c) Barnes, J. C.; Peacock, R. D. *J. Chem. Soc. A* **1971**, 558–562. (d) Li, W.; Tanner, P. A. *Inorg. Chem.* **2010**, *49*, 6384–6386. (e) Li, W.; Tanner, P. A. *Chem. Phys. Lett.* **2010**, *494*, 50–53. (f) Kirschner, A. V.; Luxbacher, T.; Fritzer, H. P.; Koppelhuber-Bitschnau, B.; Nissen, B.; Flint, C. D. *Spectrochim. Acta A* **1998**, *54*, 2045–2049.

(4) (a) Lenhert, P. G. *Acta Crystallogr.* **1980**, *36*, 1181–1183. (b) Cullen, D. L.; Lingafelter, E. C. *Inorg. Chem.* **1971**, *10*, 1264–1266. (c) Ganguly, S.; Rao, K. J.; Rao, C. N. R. *Spectrochim. Acta* **1985**, *41*, 307–314. (d) Takagi, S.; Lenhert, P. G.; Joesten, M. D. *J. Am. Chem. Soc.* **1974**, *98*, 6606–6609. (e) Reinen, D.; Friebel, C.; Reetz, K. P. *J. Solid State Chem.* **1972**, *4*, 103–114. (f) Hathaway, B. J.; Slade, R. C. *J. Chem. Soc. A* **1968**, 85–87. (g) Clack, D. W.; Reinen, D. *Solid State Commun.* **1980**, *34*, 395–399. (h) Bertrand, J. A.; Carpenter, D. A. *Inorg. Chem.* **1966**, *5*, 514–516. (i) Nakagawa, I.; Shimanouchi, T.; Yamasaki, K. *Inorg. Chem.* **1964**, *3*, 772–773. (j) Nakagawa, I.; Shimanouchi, T.; Yamasaki, K. *Inorg. Chem.* **1968**, *7*, 1332–1337. (k) Nakagawa, I. *Coord. Chem. Rev.* **1969**, *4*, 423–462. (l) Krause, R. A.; Wickenden, A. E.; Ruggles, C. R. *Inorg. Chem.* **1966**, *5*, 936–938. (m) Caulton, K. G.; Fenske, R. F. *Inorg. Chem.* **1967**, *6*, 562–568. (n) Elliott, H.; Hathaway, B. J.; Slade, R. C. *Inorg. Chem.* **1966**, *5*, 669–677.

(5) (a) Tanner, P. A. *Top. Curr. Chem.* **2004**, *241*, 167–278. (b) Duan, C.-K.; Tanner, P. A. *J. Phys. Chem. A* **2010**, *114*, 6055–6062. (c) Tanner, P. A.; Mak, C. S. K.; Faucher, M. D. *J. Chem. Phys.* **2001**, *114*, 10860–10871.

(6) Ruipérez, F.; Barandiarán, Z.; Seijo, L. *J. Chem. Phys.* **2005**, *123*, 244703–244710. Ogasawara, K.; Watanabe, S.; Toyoshima, H.; Brik, M. G. In *Handbook on the Physics and Chemistry of Rare Earths*; Gschneidner, K. A., Jr., Bünzli, J. -C., Pecharsky, V. K., Eds.; Elsevier Science BV: Amsterdam, The Netherlands, 2007; p 231. Reid, M. F.; Hu, L.; Frank, S.; Duan, C.-K.; Xia, S.; Yin, M. *Eur. J. Inorg. Chem.* **2010**, *18*, 2649–2654.

(7) Morss, L. R; Siegel, M.; Stinger, L.; Edelstein, N. *Inorg. Chem.* **1970**, *9*, 1771–1775.

(8) Brooker, M. H.; Irish, D. E. *Inorg. Chem.* **1969**, *8*, 219–223.

(9) (a) Kresse, G.; Furthmüller, J. *Phys. Rev. B* **1996**, *54*, 11169–11186. (b) Perdew, P.; Burke, K.; Ernzerhof, M. *Phys. Rev. Lett.* **1996**, *77*, 3865–3868. (c) Blöchl, P. E. *Phys. Rev. B* **1994**, *50*, 17953–17979. (d) Kresse, G.; Joubert, D. *Phys. Rev. B* **1999**, *59*, 1758–1775.

(10) (a) Hochstrasser, R. M.; Marchetti, A. P. *J. Chem. Phys.* **1969**, *50*, 1727–1736. (b) Kamada, M.; Yoshimura, T.; Kato, R. *J. Phys. Soc. Jpn.* **1977**, *42*, 1660–1668.

(11) Johnson, D. A.; Pashman, K. A. *Environ. Lett.* **1975**, *8*, 117–120.

(12) (a) Evans, A. R.; Fitchen, D. B. *Phys. Rev. B* **1970**, *2*, 1074–1091. (b) Avarmaa, R.; Rebane, L. *Phys. Status Solidi* **1969**, *35*, 107–117.

(13) (a) Faucher, M.; Garcia, D. *Phys. Rev. B* **1982**, *26*, 5451–5468. (b) Garcia, D.; Faucher, M. *J. Chem. Phys.* **1985**, *82*, 5554–5564. (c) Soulié, E. Doctoral Dissertation, Report CEA R.4849 CEN Saclay, 1977, p 28. (d) Caro, P.; Derouet, J.; Beaury, L.; Soulié, E. *J. Chem. Phys.* **1979**, *70*, 2542–2549.